Measuring the Refractive Index of a Laser-Plasma Optical System

Using laser-plasma optical systems to manipulate the basic properties of light waves has caused a recent surge of interest.[1–4] Plasma-based photonic devices are attractive because they can be ultrafast, damage resistant, and easily tunable. Alleviating concerns about optic damage by replacing conventional optics with plasma-based components could lead to the next generation of high-power, large-scale laser facilities. Plasma gratings in particular have received a great deal of attention because they are routinely used to mediate cross-beam energy transfer in indirect-drive inertial confinement fusion (ICF) experiments at the National Ignition Facility (NIF).[5–7] Multiple experiments[8,9]—including ICF experiments at the NIF[10,11]—have consistently failed, however, to observe the level of energy transfer expected on the basis of linear theory.

Recently, that theory was revisited when it was recognized that plasma gratings could also be used to dynamically control the polarization of light waves.[1] The effect of a laser-plasma system on an independent probe laser beam can be described by a complex refractive-index perturbation that is a function of the wavelength shift between the interacting beams; the system can consequently (anisotropically) modify both the phase and the amplitude of the probe and therefore act as a wave plate and/or a polarizer.[1] Turnbull *et al*. recently presented the first demonstration of a laser-plasma wave plate utilizing the system's nonzero real refractive-index perturbation that exists even in the absence of a wavelength shift between the beams. This article reports on our use of wavelength tuning to more fully map out the complete refractive-index perturbation. For the first time the real component is measured as a function of the wavelength shift. The imaginary component, which underlies cross-beam energy transfer (CBET) experiments at the NIF, is measured with sufficient accuracy to resolve both nonresonant and resonant energy transfer and is found to be in excellent agreement with linear theory (both for the first time), yielding implications for ICF experiments. The data also include the first demonstration of a laser-plasma polarizer with 85% to 87% extinction, further complementing the existing suite of plasma-based photonic devices.

Our laser-plasma optical system consists of a plasma with electron density n_e, electron temperature T_e, and ion temperature T_i, as well as a "pump" laser beam with electric field E_0 and frequency ω_0. A probe laser beam with E_1 and ω_1 will encounter resonances if $\omega_1 - \omega_0 = \pm\omega_{IAW}$; i.e., the frequency difference between the two beams is equal to the frequency of an ion-acoustic wave (IAW) with wave number $k_b = \left| \mathbf{k}_0 - \mathbf{k}_1 \right|$. The driven ion-acoustic wave mediates energy transfer between the two beams, thereby modifying the probe's amplitude. As described by the Kramers–Kronig relations, any frequency-dependent variation of the probe's amplitude in the vicinity of an optical resonance must be accompanied by variation in the real refractive index seen by the probe. The net impact of the pump on the probe beam can be described as a complex refractive-index perturbation $\delta\eta$ such that $E_1' = E_1 \exp\left(ik_1 \delta\eta L / \eta_0\right)$ after interacting with the laser-plasma system, where L is the interaction length and η_0 is the unperturbed plasma refractive index. The full expression for the refractive-index perturbation was derived in Michel *et al*.[1] using a kinetic plasma model. Critically, it was also shown in that work that the perturbation is seen only by the component of the probe's electric field that is parallel to the projection of the pump's electric field in the probe's plane of polarization (cf., Fig. 148.11). The ability to induce anisotropy via the relative orientation of the pump and probe polarizations can be exploited for precise manipulation of the probe's polarization.[1,2] Here we present measurements that show excellent agreement with linear theory for both the real and imaginary components of the refractive-index perturbation as a function of the wavelength shift between the pump and probe. Previously, the real component had been measured only at zero-wavelength shift,[2] and measurements of the imaginary component were not found to agree with linear theory.[8]

The experiment was conducted at Lawrence Livermore National Laboratory's Jupiter Laser Facility. A gas jet equipped with a 3-mm-outlet-diam supersonic nozzle released methane gas prior to the arrival of the pump and probe, which were focused over the nozzle with a relative crossing angle of 27°. Two different phase plates were used to give the pump and

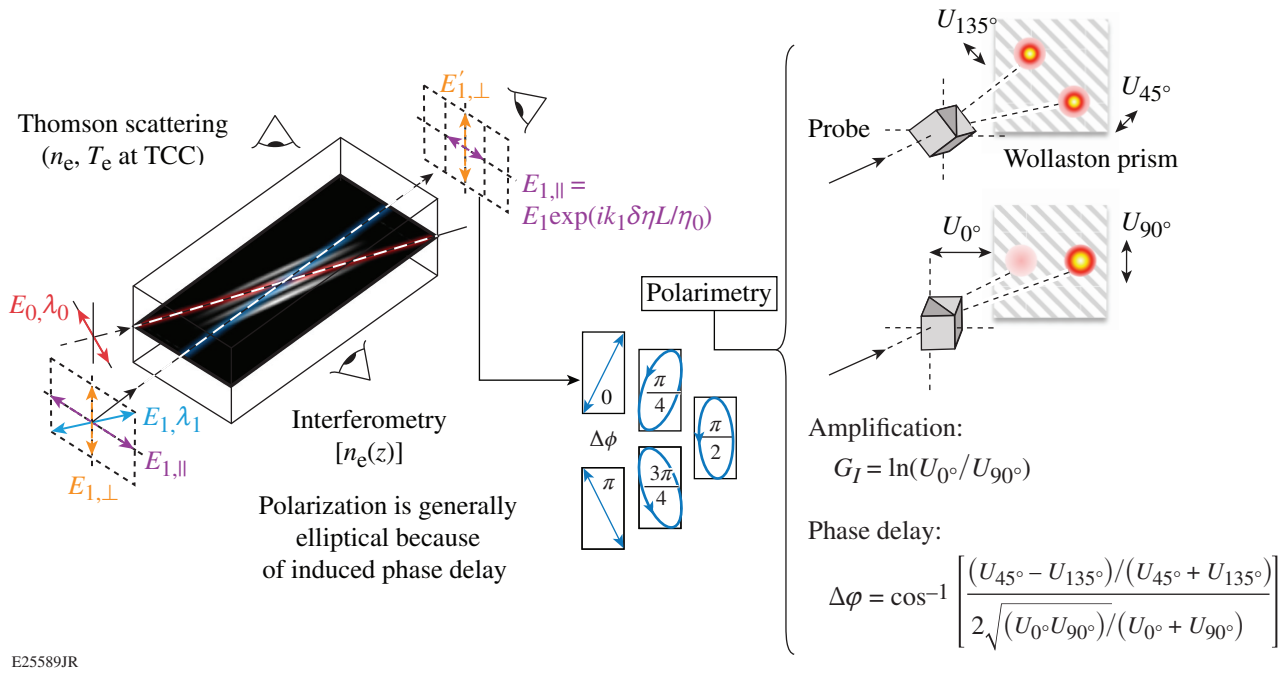

Figure 148.11
The presence of the pump introduces anisotropy to the plasma as seen by an independent probe beam. Only the component of the probe's polarization that is aligned with the pump polarization will have its amplitude and/or phase modified by the interaction, both of which can be measured using polarimetry. TCC: target chamber center.

probe speckled but roughly flattop (in an average sense) intensity distributions with 600-μm and 200-μm diameters at best focus, respectively. The pump had an ≈3-ns square pulse shape and established the plasma conditions prior to the arrival of the probe, which had an ≈250-ps Gaussian pulse shape with the peak delayed ≈1.3 ns from the rise of the pump. Using the nominal pump energies (292±8 J), fast-diode–based, pulse-shape measurements, and an assumed spot size based on the phase-plate properties, the pump intensity was expected to be in the range of $I_0 = (3.6 \pm 0.2) \times 10^{13}$ W/cm^2 averaged over the interaction region. The initial probe energy and intensity were ≈27 mJ and 3.4×10^{11} W/cm^2, respectively. Both beams used the fundamental frequency of an Nd:YLF laser ($\lambda \approx 1053$ nm), but different front ends allowed wavelength tuning within the bandwidth of the gain medium; here, a range of $-3 \le \Delta\lambda \le +3$ Å was used, where $\Delta\lambda$ is the wavelength difference between pump and probe. A polarizer was used before the last turning mirror to orient the probe polarization close to 45° relative to the horizontal pump polarization. This provides a convenient and novel method of diagnosing probe amplitude changes induced by the laser-plasma system; exploiting the anisotropic nature of the interaction, only the horizontal component of the probe's polarization will either grow or decay under the influence of the pump, and the orthogonal vertical polarization provides a baseline that factors in shot-to-shot variation of the incident probe-beam energy as well as inverse bremsstrahlung absorption in the plasma, as shown in Fig. 148.11. Separating the polarizations with a Wollaston prism subsequent to the interaction and taking their ratio provides a direct measure of the amplification. To compare with linear theory, the plasma electron density and temperature were measured with Thomson scattering. The scattered light was dominated by the high-energy pump beam, collected at a scattering angle of 90°, and directed to a streaked spectrometer measuring the blue-shifted electron plasma wave feature. To obtain additional information about density gradients in the plasma, optical interferometry was used, employing a dedicated diagnostic beam that was incident on the plasma orthogonal to the pump beam. Both diagnostics were analyzed at the time of the pump–probe interaction. The experimental setup is shown in Fig. 148.11.

The effect of the refractive-index perturbation's imaginary component can be expressed as a gain exponent G, where $E'_{1,\parallel} = E_1 \exp(G)$ and $G = k_1 \Im[\delta\eta] L/\eta_0$. Intensity being proportional to the square of the electric field, the intensity gain exponent is $G_I = 2G$ and is related to amplification, the ratio of intensity in each polarization subsequent to the interaction, by $G_I = \ln(A)$. Figure 148.12 shows the experimental data

plotted with a calculation using the linear theory developed to compute CBET in indirect-drive ICF experiments on the NIF.[5] The electron density and temperature inputs used in the calculation were $n_e/n_c = 0.0104$ and T_e = 220 eV, where n_c is the critical density, consistent with the experimentally measured values of $n_e/n_c = 0.011 \pm 0.001$, and T_e = 224±24 eV. Since several necessary inputs were not directly measured, three-dimensional radiation–hydrodynamic simulations using *HYDRA*[12] were performed to obtain estimates for ion temperature and flow velocity. The pump-beam energy, spatial profile, and pulse shape used in the simulation closely reproduced the experimental conditions, and the initial methane gas density and the flux limiter were then adjusted to match the measured electron density and temperature. The simulations predicted an ion temperature of $T_i/T_e \approx 0.09$, whereas $T_i/T_e \approx 0.12$ is used in the linear theory best fit. The small difference is comparable to the level of ion heating expected from thermalizing the energy in the driven ion-acoustic waves, which is not included in the simulations. *HYDRA* also predicts an outwardly directed radial flow resulting from the expansion of the plasma channel formed by the pump beam, which broadens the ion-acoustic resonance by shifting the peak in different portions of the interaction region; this was directly imported into the linear theory calculation because of the lack of a flow velocity measurement. The effective pump intensity was also reduced 20% from the expected value (to $I_0 = 2.9 \times 10^{13}$ W/cm^2), which we attribute to unmeasured transport losses through the final optics, inverse bremsstrahlung absorption in the plasma, pump depletion effects, and/or imperfect focusing of the pump beam. In specifying the crossing angle, the calculation takes into account the finite spread given by the *f*/6.7 and *f*/10 pump and probe beams, respectively, which also broadens the ion-acoustic resonance. Finally, the peak location of the ion-acoustic resonance was most easily matched by specifying the ion species fractions as $f_C = 0.4$ and $f_H = 0.6$, whereas $f_C = 0.2$ and f_H = 0.8 were expected based on the initial methane-gas composition. This implies that species separation is occurring in this system. In principle, hydrogen—being lighter and having a higher charge-to-mass ratio—is expected to lead the plasma channel expansion, leaving a higher concentration of carbon in the interaction region. This effect has been observed previously using simultaneous electron and ion feature Thomson scattering in an expanding CH plasma.[13,14] Assessing this effect quantitatively requires multi-ion-fluid simulations, however, and is considered outside the scope of this study. Species separation is an increasingly active field of research in the ICF community.[15–19]

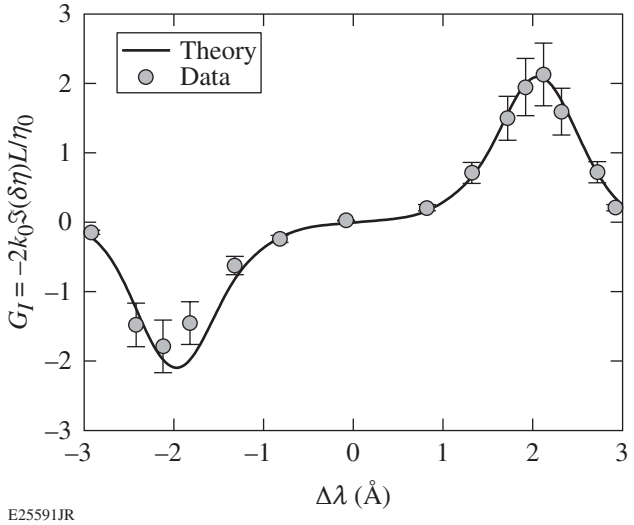

Figure 148.12
The intensity gain exponent is plotted as a function of the relative wavelength shift between the probe and pump. The parameters used in the linear theory calculation are listed in the text and are quite consistent with measured values (where available) and three-dimensional *HYDRA* simulations.

It is evident that the linear theory accurately reproduces the data both near the resonance peaks and in the off-resonant region between the Stokes and anti-Stokes peaks. Previous work utilizing a simple geometry had determined that CBET was maximized near the ion-acoustic resonance, but the peak location was not predicted accurately; the data lacked the precision to measure off-resonant transfer. It was also determined that the gain was lower than expected from the linear theory by a factor of 20 (Ref. 8). ICF hohlraums have also provided evidence that the amount of energy transfer is less than expected from linear theory.[10,11] In both previous examples, the linear theory calculations used plasma conditions taken entirely from radiation–hydrodynamic simulations. The agreement found in this better-characterized experiment suggests that inaccuracies in the assumed density and temperature may be one source of discrepancy. Weak turbulence effects associated with having many of these coupled-beam interactions in the same region of plasma may also be a factor in indirect-drive ICF.[10] Note that while the conditions of this experiment are very different from an ICF environment in terms of wavelength, intensity, density, and temperature, it can still be considered a good surrogate by several metrics. Gain was larger in this experiment than even the most resonant of interactions in an ICF hohlraum, so this can be considered an upper bound on the parameter space relevant to ICF. Furthermore, the normalized ion-acoustic–wave damping is $\nu/\omega_{IAW} \approx 0.1$ to 0.2 (i.e., strongly damped) in both cases; achieving this in the present experiment motivated the use of the multispecies methane gas.[20]

As mentioned, the imaginary refractive-index perturbation component is accompanied by a real refractive-index change, which introduces a phase delay between the probe's vertical (noninteracting) and horizontal (interacting) components. While amplification was determined by separating the vertical and horizontal components and taking their ratio (which is insensitive to the phase delay), inferring the phase delay $\Delta\phi$ requires a second measurement in which the Wollaston prism is rotated 45° in order to separate the 45° and 135° polarization components. With each signal's energy in arbitrary units given by U_j, where j is the polarization angle, the phase delay for each pair of measurements (assuming polarized light and perfect shot-to-shot reproducibility) is given by

$$\Delta\phi = \cos^{-1}\left[\frac{\left(U_{45^\circ} - U_{135^\circ}\right)\Big/\left(U_{45^\circ} + U_{135^\circ}\right)}{2\sqrt{U_{0^\circ}U_{90^\circ}}\Big/\left(U_{0^\circ} + U_{90^\circ}\right)}\right]. \qquad (1)$$

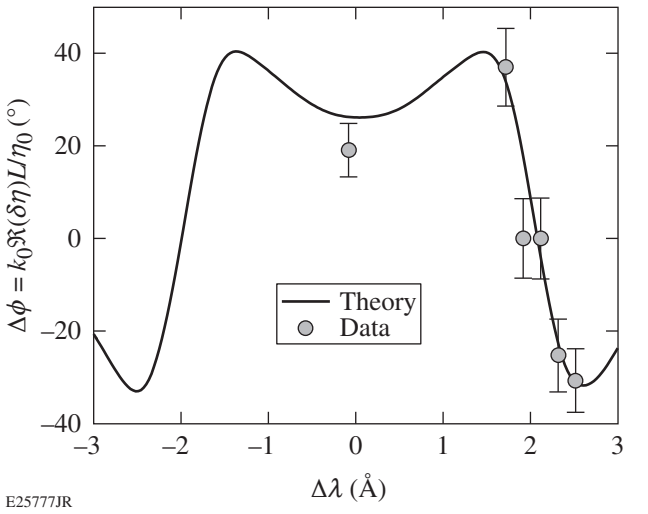

Figure 148.13
The phase delay induced by the real refractive-index perturbation is plotted as a function of the wavelength shift between the pump and probe. The linear theory is once again in good agreement with the experimental data.

Unlike the imaginary component, the real component of the refractive-index perturbation is nonzero even in the absence of a wavelength shift between the pump and probe. Turnbull *et al*. exploited this property previously in the first demonstration of a laser-plasma wave plate, converting an initially elliptical polarization into a nearly ideal circular polarization.[2] Here, wavelength tuning capability allows us to validate other points along the real refractive-index perturbation curve, as shown in Fig. 148.13. Again, the linear theory provides a good match to the experimental data using the same parameters that were used to fit the amplification data, with key features—nonzero phase delay at zero wavelength shift, larger dephasing on either side of the resonance, and zero dephasing at the peak—evident in the data. Note that the measurement does not actually discriminate between positive and negative phase delay, but since the data are consistent with the shape of the curve as predicted by linear theory, we assume that those points to the left of the peak are positive and points to the right of the peak are negative. This is the first (to our knowledge) measurement of a laser-plasma optical system's real refractive-index perturbation as a function of wavelength tuning.

The experiment was designed in such a way to test the concept of a "plasma polarizer," which was proposed by Michel *et al*.[1] When $\lambda_1 - \lambda_0 < 0$, the probe transfers energy to the pump but only out of its horizontal component (which is aligned with the pump polarization) resulting from the anisotropy of the laser-plasma system, so the system is effectively a linear polarizer. The data point at the negative peak of Fig. 148.12 represents an extinction of 85%. The data are shown in Fig. 148.14; the incident polarization was oriented in order to have nearly equal horizontal and vertical components, but after propagating through the system, the horizontal polarization is significantly attenuated. Additional shots were conducted in which the incident probe intensity was increased up to $I_1 \approx 3 \times 10^{12}$ W/cm^2, and the extinction stayed in the range of 85% to 87%. Note that the probe is otherwise minimally affected by the system because the phase delay induced between the vertical polarization and what is left of the horizontal polarization is close to zero near the resonance peak, absorption in this fairly tenuous plasma is calculated to be modest, and the probe is not degraded by other laser–plasma instabilities. Maintaining similar plasma conditions, the extinction could be increased or decreased by changing the pump intensity. This demonstrates another ultrafast, damage-resistant, and tunable laser-plasma photonic device. Having now achieved both a wave plate and a polarizer, it is possible to design a laser Q switch using only laser-plasma systems.

In summary, a laser-plasma optical system's complete refractive index—both its imaginary and real components—was mapped out for the first time, using a consistent set of laser and plasma parameters. It was found to be in excellent agreement with the linear theory for coupled beams in a plasma that is used to compute cross-beam energy transfer in indirect-drive ICF experiments. The ability to correctly predict energy transfer in this well-characterized context, but not in ICF experiments,[10,11] points to possible errors in the hydrodynamic inputs to the ICF

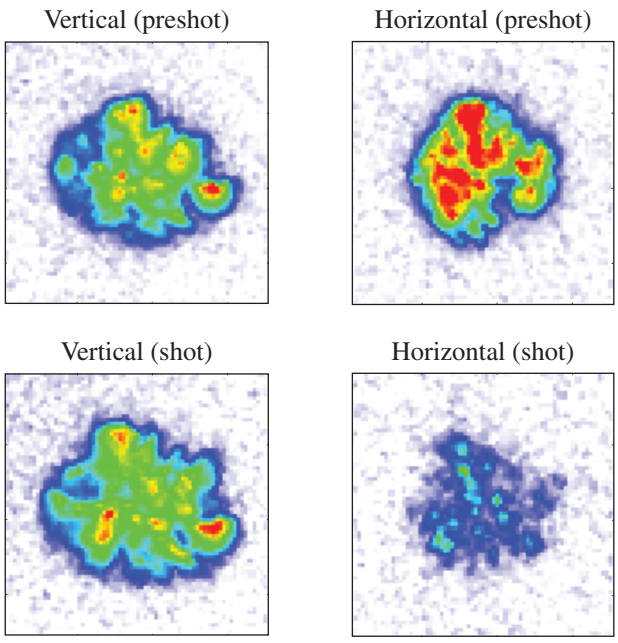

Figure 148.14
The anisotropic laser-plasma system acts like a pure linear polarizer at the negative resonance peak, depleting the probe's horizontal polarization component. The color scale for each pair is normalized to the vertical polarization. The vertical and horizontal spots appear to be different because the Wollaston prism slightly affects the imaging. The pre-shot images were obtained without any plasma, and the horizontal polarization was brighter than the vertical polarization because the polarizer setting the incident polarization was not quite oriented at 45°; 85% to 87% of the horizontal polarization was then extinguished by the laser-plasma polarizer, whereas the vertical polarization was minimally perturbed by the system.

calculations and/or weak turbulence effects from having many such coupled beam interactions in the same volume of plasma. We also achieved the first demonstration of a laser-plasma polarizer, which extinguished 85% to 87% of an independent probe beam's horizontal polarization.

ACKNOWLEDGMENT

This work was performed under the auspices of the U.S. Department of Energy by Lawrence Livermore National Laboratory under Contract DE-AC52-07NA27344. This work was supported by the LLNL-LDRD Program under Project No. 42074. We thank the staff of the Jupiter Laser Facility and Suzanne Ali for enabling a successful experimental campaign. DT also acknowledges useful discussions regarding species separation with C. Bellei, P. Amendt, and G. Kagan.

REFERENCES

1. P. Michel, L. Divol, D. Turnbull, and J. D Moody, Phys. Rev. Lett. **113**, 205001 (2014).
2. D. Turnbull, P. Michel, T. Chapman, E. Tubman, B. B Pollock, C. Y. Chen, C. Goyon, J. S Ross, L. Divol, N. Woolsey, and J. D Moody, Phys. Rev. Lett. **116**, 205001 (2016).
3. D. J. Stark *et al*., Phys. Rev. Lett. **115**, 025002 (2015).
4. G. Lehmann and K. H. Spatschek, Phys. Rev. Lett. **116**, 225002 (2016).
5. P. Michel *et al*., Phys. Rev. Lett. **102**, 025004 (2009).
6. S. H. Glenzer *et al*., Science **327**, 1228 (2010).
7. J. D. Moody *et al*., Nat. Phys. **8**, 344 (2012).
8. R. K. Kirkwood *et al*., Phys. Rev. Lett. **76**, 2065 (1996).
9. R. K. Kirkwood, J. D. Moody, A. B. Langdon, B. I. Cohen, E. A. Williams, M. R. Dorr, J. A. Hittinger, R. Berger, P. E. Young, L. J. Suter, L. Divol, S. H. Glenzer, O. L. Landen, and W. Seka, Phys. Rev. Lett. **89**, 215003 (2002).
10. P. Michel *et al*., Phys. Rev. Lett. **109**, 195004 (2012).
11. R. P. J. Town *et al*., Phys. Plasmas **18**, 056302 (2011).
12. M. M. Marinak *et al*., Phys. Plasmas **8**, 2275 (2001).
13. J. S. Ross *et al*., Rev. Sci. Instrum. **83**, 10E323 (2012).
14. P. Amendt *et al*., Phys. Rev. E **91**, 023103 (2015).
15. J. R. Rygg, J. A. Frenje, C. K. Li, F. H. Séguin, R. D. Petrasso, J. A. Delettrez, V. Yu. Glebov, V. N. Goncharov, D. D. Meyerhofer, S. P. Regan, T. C. Sangster, and C. Stoeckl, Phys. Plasmas **13**, 052702 (2006).
16. G. Kagan and X.-Z. Tang, Phys. Plasmas **19**, 082709 (2012).
17. C. Bellei and P. A. Amendt, Phys. Rev. E **90**, 013101 (2014).
18. M. J. Rosenberg, A. B. Zylstra, F. H. Séguin, H. G. Rinderknecht, J. A. Frenje, M. Gatu Johnson, H. Sio, C. J. Waugh, N. Sinenian, C. K. Li, R. D. Petrasso, P. W. McKenty, M. Hohenberger, P. B. Radha, J. A. Delettrez, V. Yu. Glebov, R. Betti, V. N. Goncharov, J. P. Knauer, T. C. Sangster, S. LePape, A. J. Mackinnon, J. Pino, J. M. McNaney, J. R. Rygg, P. A. Amendt, C. Bellei, L. R. Benedetti, L. Berzak Hopkins, R. M. Bionta, D. T. Casey, L. Divol, M. J. Edwards, S. Glenn, S. H. Glenzer, D. G. Hicks, J. R. Kimbrough, O. L. Landen, J. D. Lindl, T. Ma, A. MacPhee, N. B. Meezan, J. D. Moody, M. J. Moran, H.-S. Park, B. A. Remington, H. Robey, M. D. Rosen, S. C. Wilks, R. A. Zacharias, H. W. Herrmann, N. M. Hoffman, G. A. Kyrala, R. J. Leeper, R. E. Olson, J. D. Kilkenny, and A. Nikroo, Phys. Plasmas **21**, 122712 (2014).
19. H. G. Rinderknecht, M. J. Rosenberg, C. K. Li, N. M. Hoffman, G. Kagan, A. B. Zylstra, H. Sio, J. A. Frenje, M. Gatu Johnson, F. H. Séguin, R. D. Petrasso, P. Amendt, C. Bellei, S. Wilks, J. Delettrez, V. Yu. Glebov, C. Stoeckl, T. C. Sangster, D. D. Meyerhofer, and A. Nikroo, Phys. Rev. Lett. **114**, 025001 (2014).
20. E. A. Williams *et al*., Phys. Plasmas **2**, 129 (1995).